THE JOURNAL OF PHYSICAL CHEMISTRY A

Article

Cite This: J. Phys. Chem. A 2019, 123, 3647−3654

pubs.acs.org/JPCA

Quantum Suppression of Intramolecular Deuterium Kinetic Isotope Effects in a Pericyclic Hydrogen Transfer Reaction

Xiao Li,[†] Darrin M. York,*[,†] and Matthew P. Meyer*[,‡]

[†]Laboratory for Biomolecular Simulation Research, Center for Integrative Proteomics Research, and Department of Chemistry and Chemical Biology, Rutgers University, Piscataway, New Jersey 08854-8087, United States

[‡]Department of Chemistry and Chemical Biology, University of California, Merced, California 95343, United States

Supporting Information

ABSTRACT: It is generally accepted that hydrogen tunneling enhances both primary and secondary H/D kinetic isotope effects (KIEs) over what would be expected under the assumptions of classical barrier transition. Previous studies have exclusively shown that the effects of tunneling upon primary H/D KIEs have been much larger than those observed for secondary H/D KIEs. Here we present a series of experimental H/D KIE results associated with the Chugaev elimination of methyl xanthate derived from β-phenylethanol over the temperature range of 180 to 290 °C. Intramolecular H/D KIEs computed according to classical transition state theory (TST) are markedly overestimated relative to experimentally measured values. Experimental intermolecular H/D KIEs and direct dynamic calculations based on canonical variational transition state theory (CVT) with small-curvature tunneling correction (SCT) reveal that this result is largely the consequence of extraordinary tunneling enhancement of the *secondary* H/D KIE. This unexpected behavior is examined in the context of other similar hydrogen transfer reactions.

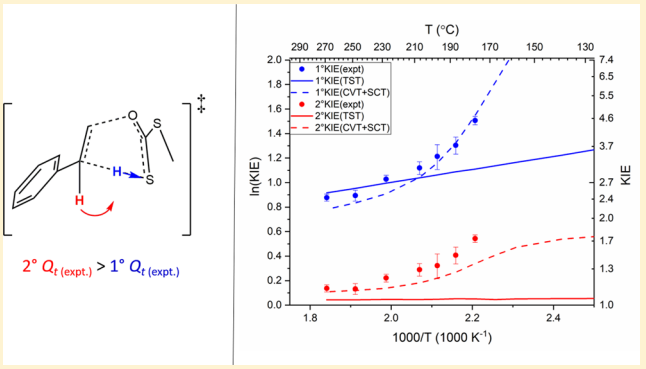

1. INTRODUCTION

Hydrogen tunneling has generated a lot of debate within the chemical and biochemical communities.[1−5] This is because hydrogen transfer is important to numerous synthetically useful transformations and the vast majority of biological processes, while the effects of tunneling upon hydrogen transfer remain poorly understood in many reactions. Quantum mechanical tunneling exhibits phenomena that cannot be accounted for using classical transition state theory (TST), which is the most generally applicable theory for chemical kinetics within the classical regime.[6,7] Cogent models exist for proton-coupled electron transfer reactions that yield extremely large primary deuterium KIEs[8,9] and for atom−diatomic collinear reactions.[10,11] Surprisingly, the quantum mechanical behavior of hydrogen remains poorly understood for many heterolytic polyatomic hydrogen transfer reactions. This knowledge gap hinders our ability to understand reactivity and selectivity in reactions significant to both metabolism and chemical synthesis. Improved models for reactions that exhibit significant influence from quantum mechanical tunneling promise to facilitate improved enzyme inhibitors for small molecule drug design and better catalysts for reactions involving hydrogen transfer.[12−14] Before better models can be constructed for reactions that involve substantial quantum behavior, an expanded set of well-interpreted experimental results needs to be presented. This paper is intended to present a model system in which common metrics for tunneling indicate classical behavior that masks surprising nonclassical behavior.

This work studies the tunneling effect in the intramolecular syn-β-elimination reaction in *S*-methyl *O*-(2-phenyl)ethyl xanthate **1** (Scheme 1) by examining the temperature dependence of the KIEs through both experiments and calculations. Kinetic isotope effects are often the observable chosen to demonstrate the importance of tunneling in a given reaction.[15−22] Efforts over the past couple of decades have attempted to unite a conceptual view of hydrogen tunneling with both magnitudes and temperature dependencies of KIEs.

Scheme 1. Chugaev Elimination

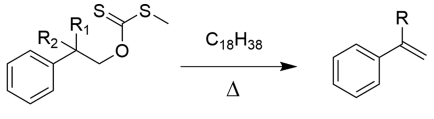

1, $R_1 = R_2 = H$
D_1-**1**, $R_1 = H$, $R_2 = D$
D_2-**1**, $R_1 = R_2 = D$

2, R = H
D_1-**2**, R = D

Received: January 7, 2019
Revised: March 9, 2019
Published: March 11, 2019

DOI: 10.1021/acs.jpca.9b00172
J. Phys. Chem. A 2019, 123, 3647−3654

In spite of extensive work, a consensus has not been reached concerning the strange temperature dependencies of primary deuterium KIEs observed in some enzymatic systems.[23−25] Although progress have been made toward a conventional wisdom regarding the temperature dependence of KIEs in tunneling systems, new findings continue to challenge our working models.

Our experimental results show that the Chugaev elimination of **1** exhibits a deceptively classical Arrhenius plot of the intramolecular H/D KIE that masks intrinsically nonclassical behavior of the primary and secondary KIEs. These results challenge commonly accepted expectations by demonstrating that (1) tunneling can have profound influence upon isotope effects measured at temperatures well in excess of room temperature and (2) that secondary KIEs can be inflated by tunneling to a *greater* degree than primary KIEs. Computational modeling of the Chugaev elimination using canonical variational transition state theory (CVT) in conjunction with small-curvature tunneling (SCT) correction for quantum barrier crossing replicate the experimental results to a reasonable degree of qualitative and quantitative fidelity.

2. RESULTS AND DISCUSSION

2.1. Intramolecular KIEs. The intramolecular KIE, k_{HD}/k_{DH}, for the Chugaev elimination of D_1-**1** were measured by quantifying the resulting isotopic product distribution of D_1-**2** vs **2** (eq 1) using quantitative ^{1}H NMR. The first letter in the subscript of k_{HD} indicates the transferred Hydron, and the second letter indicates the retained Hydron.

$$\mathrm{KIE}_{Intra} = \frac{1°\mathrm{KIE}}{2°\mathrm{KIE}} = \frac{D_1\text{-}\mathbf{2}}{\mathbf{2}} \quad (1)$$

The Arrhenius-type plot of $\ln(\mathrm{KIE}_{intra})$ over $1000/T$ is displayed in Figure 1. The temperature dependence of measured intramolecular KIE over 180 to 290 °C is $k_{HD}/k_{DH} = 0.76\exp(1.08\ \mathrm{kcal{\cdot}mol^{-1}}/RT)$. At 190 °C, the intramolecular KIE is 2.45 ± 0.04. Extrapolated to 25 °C, this KIE is 4.02. By

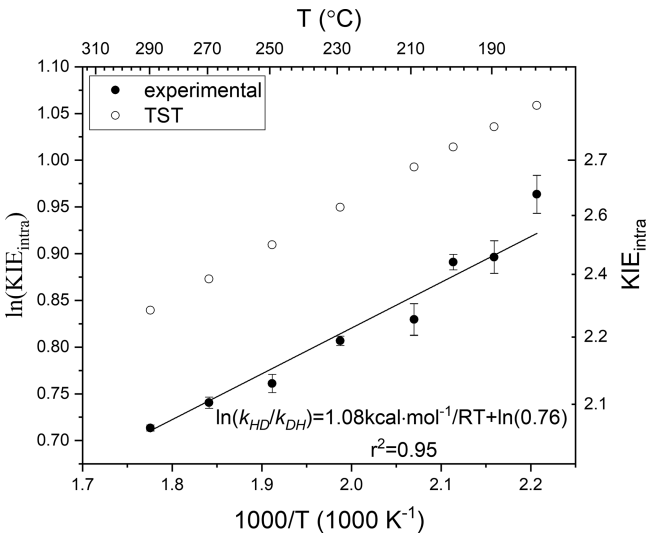

Figure 1. Arrhenius plot of $\ln(\mathrm{KIE}_{intra})$ vs $1000/T$ for experimental and computational intramolecular KIE at 290, 270, 250, 230, 210, 200, 190, and 180 °C. The linear fit information is shown on the graph. The computational KIEs are computed by POLYRATE with GAUSSRATE interface to Gaussian with TST method, at M06-2*X*/6-31+G(d,p) level of theory, with SMD heptane solvation.

definition, the intramolecular KIE for C−H cleavage from a methylene carbon is the ratio of the primary to the secondary KIE (eq 1). Even if one assumes a substantial 2° H/D KIE of approximately 1.2, which is typically associated with late, product-like transition states in processes like solvolysis, the primary H/D KIE at 25 °C could be assigned a maximal value of 4.83.[26]

The experimental intramolecular KIE results indicate: the ratio of the pre-exponential factors ($A_{HD}/A_{DH} = 0.76$) is within the classical range ($0.7\sim\sqrt{2}$), the difference in the activation energy ($\Delta\Delta E = \Delta E_{DH} - \Delta E_{HD} = 1.08\ \mathrm{kcal{\cdot}mol^{-1}}$) is small, and the KIE values are moderate. According to classic works by Bell,[7] Stern,[27] and Weston,[28] these values do not make a convincing case that hydrogen tunneling is a dominant or even substantial factor in the Chugaev elimination.

It could be argued that the experimental data in Figure 1 possess a small degree of upward concave curvature. However, the confidence with which concavity may be imputed is questionable. It is noteworthy that the computed KIEs using TST method *exceed* experimental values by a significant margin, e.g., the computed intramolecular KIE at 190 °C is 2.82. This trend runs contrary to what is most frequently observed, where calculations based on TST with no tunneling correction typically yield smaller KIEs than experimental values, where tunneling is thought to have even the smallest influence.[29] Computational overestimation of intramolecular KIEs in the Chugaev elimination led us to interrogate this system further.

2.2. Primary and Secondary KIEs. For systems in which the rate- and product-determining steps are identical, the intramolecular and intermolecular KIEs can be used to solve for primary (1°) and secondary (2°) KIEs for hydrogen transfer reactions at a methylene group. The intermolecular KIE that reflects the relative elimination rates between **1** and D_1-**1** is a function of the 1° and 2° KIEs as shown in eq 2. Equations 1 and 2 can be solved simultaneously to yield expressions of the primary and secondary H/D KIEs (eqs 3 and 4), even though these values cannot be directly measured. (Refer to the Supporting Information, section III-(iv) for derivation.)

$$\mathrm{KIE}_{Inter} = \frac{2}{1/1°\mathrm{KIE} + 1/2°\mathrm{KIE}} \quad (2)$$

$$1°\mathrm{KIE} = \frac{\mathrm{KIE}_{Inter}(1 + \mathrm{KIE}_{Intra})}{2} \quad (3)$$

$$2°\mathrm{KIE} = \frac{\mathrm{KIE}_{Inter}(1 + 1/\mathrm{KIE}_{Intra})}{2} \quad (4)$$

Extracting primary and secondary KIEs and using eqs 3 and 4 from 180 to 270 °C yields the Arrhenius plots shown in Figure 2. Values computed by POLYRATE[30] using TST and CVT+SCT methods are also shown for comparison. These data are noteworthy for three reasons. First, nearly equivalent upward concave curvature is evident in the Arrhenius plots of both primary and secondary KIEs. As nonlinear, curved temperature dependence of ln(KIE) is one important indicator of tunneling,[31] our results indicate significant tunneling effect. Second, the magnitudes of the KIEs, especially secondary KIEs, extend beyond what might be expected in a reaction with behavior which is consonant with transition state theory. At the lower-temperature-end, both primary and secondary KIEs substantially exceed the values predicted by TST (solid lines in

DOI: 10.1021/acs.jpca.9b00172
J. Phys. Chem. A 2019, 123, 3647−3654

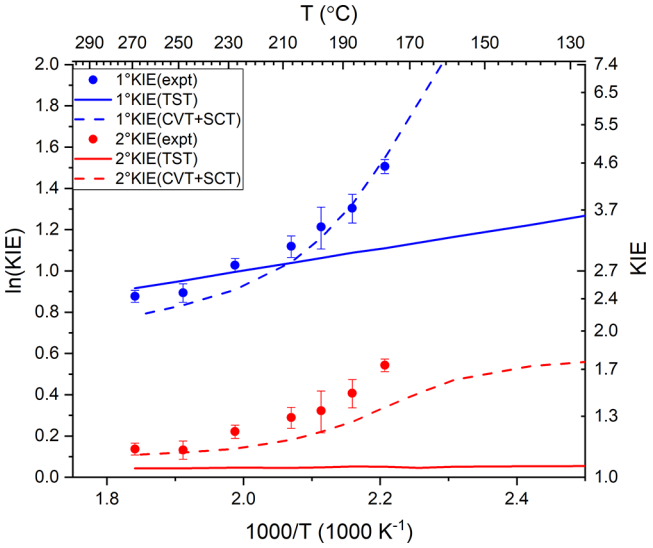

Figure 2. Arrhenius plots of ln(KIE) vs 1000/T for experimental and computational primary and secondary KIEs. Experimental KIEs are plotted at 270, 250, 230, 210, 200, 190, and 180 °C. Computational results are calculated by POLYRATE with GAUSSRATE interface to Gaussian, with TST or CVT+SCT method, at the M06-2X/6-31+G(d,p) level of theory, with SMD heptane solvation.

Figure 2). This result is due to the relatively greater impact tunneling has at lower temperatures. What is surprising is the magnitude of the secondary KIE at 180 °C (1.72)! To our knowledge, this is among the largest secondary KIE measured. The fact that this substantial secondary KIE occurs at far above room temperature and is exalted to a greater degree than the primary KIE at the same temperature challenges the notions that only transferred hydrogenic positions can dominate the tunneling event and that tunneling phenomena are influential only at room temperature or below.

Finally, POLYRATE Computation with canonical variational transition state theory (CVT) and small-curvature tunneling correction (SCT) reproduced the concaved temperature dependence of the ln(KIE) vs 1000/T (Figure 2), which will be discussed in the following sections.

2.3. Analysis of the Rule of Geometric Mean. The intermolecular KIE between **1** and D_2-**1** was measured to examine the rule of geometric mean (RGM). According to RGM, the KIE of a doubly labeled species should be the product of the primary and secondary KIEs (eq 5) when tunneling has little influence upon the reaction in question.[32,33] Substantial violation of RGM is suggestive of the presence of significant tunneling effect in the reaction.[34,35] At 190 °C, KIE_{inter_DD} was measured to be 6.6 ± 0.1. At the same temperature, 1° KIE × 2° KIE = (3.67 ± 0.25) × (1.50 ± 0.10) = 5.51 ± 0.52. The product of primary and secondary KIEs is significantly different from the dideuterated KIE, deviating from RGM and thus consistent with tunneling.

$$\text{RGM: } KIE_{inter\_DD} = \frac{k_{HH}}{k_{DD}} = \frac{k_{HH}}{k_{DH}}\cdot\frac{k_{HH}}{k_{HD}} = 1°\text{KIE} \times 2°\text{KIE} \quad (5)$$

It is worth mentioning that **1** and its isotopologs are shelf stable at room temperature and undergo Chugaev elimination with reportedly no other side reactions when heated (see Supporting Information, section V). The mechanism of Chugaev elimination has been well established, in which the thion sulfur abstracts a β-hydrogen via a cyclic transition state in the rate-limiting step. Previous S^{32}/S^{34} and C^{12}/C^{13} KIE studies have ruled out the rearrangement pathway of the xanthate under the reaction conditions.[36,37] The ^{2}H NMR on p S30 also indicate no PhCH2CH2SCOSMe isomer present. Nonetheless, based on the experiments conducted here, one cannot definitively eliminate the possibility that there could be alternative pathways available that lead to side reactions that were not detected.

2.4. Computational Studies. Initial efforts to model the temperature dependence of the 1° and 2° H/D KIEs associated with the Chugaev elimination failed to reproduce observed trends both qualitatively and quantitatively. If, as Figure 1 and Figure 2 suggested, the 2°KIE was exceptionally

Table 1. Experimental and Computational Primary and Secondary KIEs for the Chugaev Elimination Reaction

	1° KIE					1° Q_t		
T (°C)	experimental	TST	CVT	TST+W[a]	CVT+SCT	1° $Q_{t\ (expt/TST)}$[b]	1° $Q_{t\ (W)}$[c]	1° $Q_{t\ (SCT)}$[d]
180	4.51 ± 0.15	3.03	2.25	3.30	4.70	1.49	1.085	2.02
190	3.67 ± 0.25	2.97	2.20	3.21	3.75	1.24	1.082	1.65
200	3.36 ± 0.34	2.89	2.15	3.12	3.19	1.16	1.079	1.42
210	3.06 ± 0.16	2.83	2.12	3.04	2.84	1.08	1.077	1.29
230	2.80 ± 0.09	2.71	2.04	2.90	2.48	1.03	1.072	1.16
250	2.44 ± 0.11	2.59	1.98	2.77	2.30	0.94	1.067	1.11
270	2.40 ± 0.07	2.50	1.92	2.65	2.19	0.96	1.063	1.09
	2° KIE					2°Q_t		
T (°C)	experimental	TST	CVT	TST+W[a]	CVT+SCT	2° $Q_{t\ (expt/TST)}$[b]	2° $Q_{t\ (W)}$[c]	2° $Q_{t\ (SCT)}$[d]
180	1.72 ± 0.05	1.05	1.12	1.07	1.40	1.63	1.015	1.26
190	1.50 ± 0.10	1.05	1.11	1.06	1.31	1.42	1.014	1.18
200	1.38 ± 0.14	1.05	1.11	1.06	1.25	1.32	1.014	1.12
210	1.34 ± 0.07	1.05	1.11	1.06	1.20	1.28	1.013	1.08
230	1.25 ± 0.04	1.05	1.11	1.06	1.15	1.19	1.013	1.04
250	1.14 ± 0.05	1.04	1.11	1.06	1.13	1.09	1.012	1.02
270	1.15 ± 0.03	1.04	1.10	1.06	1.12	1.10	1.011	1.01

[a] KIE^{TST+W} is KIE calculated with Wigner tunneling correction at TST level, $k^{TST+W} = \kappa^W \cdot k^{TST}$. [b] $Q_{t(expt/TST)} = KIE^{expt}/KIE^{TST}$. [c] 1° $Q_{t\ (W)} = \kappa^W_{HH}/\kappa^W_{DH}$; 2°$Q_{t\ (W)} = \kappa^W_{HH}/\kappa^W_{HD}$. [d] 1° $Q_{t\ (SCT)} = \kappa^{SCT}_{HH}/\kappa^{SCT}_{DH}$; 2°$Q_{t\ (SCT)} = \kappa^{SCT}_{HH}/\kappa^{SCT}_{HD}$.

DOI: 10.1021/acs.jpca.9b00172
J. Phys. Chem. A 2019, 123, 3647−3654

exalted by tunneling, we would need to employ an approach that is inherently multidimensional. Toward that end, we employed POLYRATE[30] with GAUSSRATE[38] interface to Gaussian 09[39] using the M06-2X[40]/6-31+G(d,p)[41] functional to compute rate constants and transmission coefficients as a function of isotopolog. Results under the assumptions of transition state theory (TST) and canonical variational transition state theory (CVT)[42,43] were obtained. Multidimensional tunneling corrections were calculated using small-curvature tunneling (SCT)[44,45] option in POLYRATE. Some computational results are plotted in Figures 1 and 2, while more results are tabulated in Table 1. Three major observations can be drawn from the computational results.

First, CVT+SCT calculation reproduces experimental results in magnitude better than TST. As shown in Figure 2, compared to TST method, CVT+SCT method generates smaller 1° KIE values at higher temperatures, greater 1° KIE values at lower temperatures, and greater 2° KIEs, approaching more closely to the experimental values. Despite that SCT is the dominate factor, CVT without any tunneling correction starts to correct the rate constant toward the right direction (Table 1). CVT generates larger 2° KIE and smaller 1° KIE values than TST. The accurate approximation of the nontunneling rate constant is the first step toward the overall accuracy of the rate constant, as tunneling correction is a multiplicative term to the semiclassical rate constant calculated based on either TST or CVT. For example, rate constant calculated with CVT+SCT is the product of CVT rate constant (k^{CVT}) and SCT transmission coefficient kappa (κ^{SCT}) (eq 6). Canonical variational theory (CVT) is known to correct the conventional

$$k^{CVT+SCT} = \kappa^{SCT} \cdot k^{CVT} \tag{6}$$

transition state theory (TST) by including zero-point energy and entropic effects. The location of the CVT transition state is the structure with the highest free energy while TST saddle point is the structure with the highest potential energy along the MEP.[46]

Second, CVT+SCT calculations successfully predict the concave-up trend of ln(KIE) vs 1000/T for both primary and secondary KIEs. SCT tunneling correction reproduces the temperature dependence of primary and secondary KIEs better than other theories. As can be seen from Table 1, SCT correction term $Q_{t(SCT)}$ is the major contributor to the inflation of the KIE values at lower temperatures, and is responsible to the curvature of the KIEs. As a comparison, the one-dimensional Wigner tunneling correction ($Q_{t(W)}$) fails to predict either the magnitude or the trend for primary and secondary KIEs. The large curvature tunneling (LCT) calculation is useful for systems where the tunneling reaction path is close to a straight line from the reactant to the product valley.[47,48] However, the LCT method was not found to be the dominant tunneling mechanism in the Chugaev elimination reaction as it did not increase the transmission coefficient beyond SCT method. This is not unusual among other hydrogen transfer reactions.[19,49,50]

The third observation from POLYRATE calculation is that CVT+SCT calculation has limitations in predicting the tunneling effect on 2° KIEs. While experimental quantum amplification in 2° KIE is greater than that in 1° KIE (2° $Q_{t(expt/TST)}$ > 1° $Q_{t(expt/TST)}$), SCT calculation predicts the contrary (2° $Q_{t\ (SCT)}$ < 1° $Q_{t\ (SCT)}$).

To understand the tunneling behavior observed in the Chugaev elimination better, we examine the transition structures. The reactant **1** and the TST saddle point are optimized by Gaussian 09 at M06-2X/6-31+G(d,p) level of theory with SMD solvent model for heptane, and the structures are shown in Figure 3. The distance between the transferred hydrogen (H_{13}) and the acceptor sulfur (S_{21}) is denoted as r_1. The distance between C_{15} and O_{18} that undergoes bond breaking is denoted as r_2. The dihedral angle involving the hydrogen donor carbon (C_{12}) that undergo sp^3 to sp^2 rehybridization are denoted as d_1. r_1, r_2, and d_1 are labeled and highlighted in Figure 3, and the values are tabulated in Table 2.

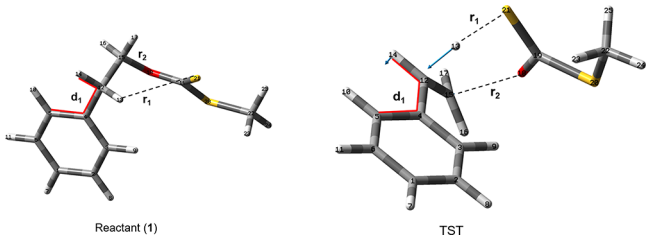

Figure 3. M06-2X/6-31+G(d,p) structures of the reactant (**1**) and the TST saddle point with key metrics labeled. r_1 and r_2 denotes bond S_{21}–H_{13} and C_{15}–O_{18} respectively. Dihedral angle of H_{14}–C_{12}–C_4–C_5 is outlined in red and labeled as d_1. The displacement vector of the imaginary frequency (952.65i cm^{-1}) of the saddle point is shown by blue arrows. The CVT transition structure is very close to the TST saddle point (see Table 2).

Table 2. Selected Bond Lengths, Bond Orders and Dihedral Angle in the Reactant (1), TST Saddle Point, and the CVT Transition Structure

	r_1 (Å)	r_2 (Å)	n_1[b]	n_2[b]	d_1 (deg)
1	2.91	1.44	0.00[c]	1.00	39.3
TST	1.74	2.04	0.52	0.37	3.4
CVT[a]	1.82	2.01	0.45	0.39	0.1

[a]CVT transition structure at 180 °C. [b]Bond order, $n_i = \exp\left[\frac{(r_i^0 - r_i)}{C}\right]$ where r_i^0 is the single bond length in the reactant or product in angstrom, and C = 0.6 Å. [c]No bonding between S_{21} and H_{13} in **1**. r_1^0 = 1.34 Å in the product CH_3SCOSH is used in calculation of n_1 for the saddle point and the CVT structure.

In addition, the key metrics of the CVT transition structure at 180 °C are also listed in Table 2. The bond order (n_i) corresponds to a certain interatomic distance (r_i) is calculated through Pauling relation[51] in eq 7, where r_i^0 is the single bond length in the reactant or the product, r_i^0 and r_i have a unit in angstrom, and C = 0.6 Å.[52] The TST saddle point and CVT transition state are placed on a More O'Ferrall-Jencks diagram in Figure 4, in which the x-axis is the degree of bond formation of S_{21}–H_{13} bond, and the y-axis is the degree of C_{15}–O_{18} bond breaking.

$$n_i = \exp\left[\frac{r_i^0 - r_i}{C}\right] \tag{7}$$

The CVT transition structure is located more toward the reactant side compared to the saddle point on the reaction coordinate according to POLYRATE calculation, which is also

DOI: 10.1021/acs.jpca.9b00172
J. Phys. Chem. A 2019, 123, 3647−3654

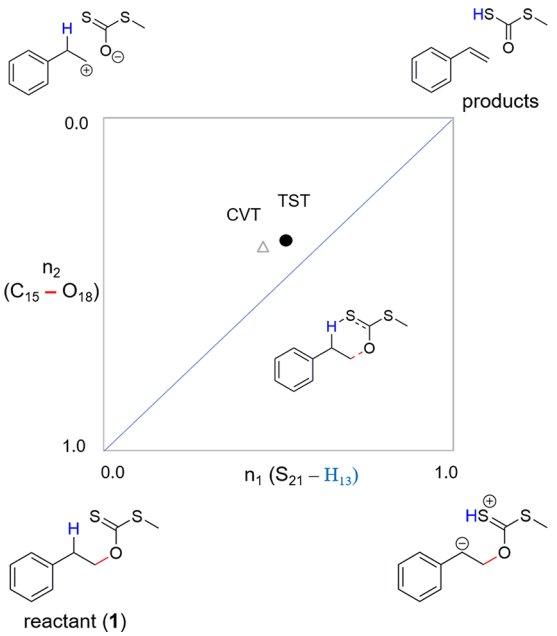

Figure 4. More O'Ferrall–Jencks diagrams for the Chugaev elimination of **1**. The solid circle represents the position of the TST saddle point, and the open triangle represents the position of CVT transition structure. Transition state positions are calculated from bond orders of S_{21}–H_{13} (n_1) and C_{15}–O_{18} (n_2) (values in Table 2). A diagonal line connecting the reactant and products is shown. The intermediate structures of two extreme scenarios: complete S_{21}–H_{13} breakage and complete C_{15}–O_{18} formation are shown in the lower-right and upper-left corners. The transition structure with partial S_{21}–H_{13} breakage and C_{15}–O_{18} formation in shown on the diagram.

reflected in the More O'Ferrall–Jencks diagram (Figure 4). The CVT transition structure has less formation of S_{21}–H_{13} bond and less breakage of C_{15}–O_{18} bond (Figure 4 and Table 2), resembling the reactant more in terms of bond breaking/making. However, the dihedral angle d_1 is more planar in the CVT transition structure (Table 2), which indicates a more advanced sp^3 to sp^2 rehybridization at the C_{12} center, meaning the CVT structure resembles the product more than the TST structure in terms of rehybridization of C_{12}. These features align with the KIE values in Table 1: Compared to the TST method, the CVT method computes smaller 1° KIEs and greater 2° KIEs, corresponding to a less bond breaking/making but more rehybridized CVT transition structure.

The imaginary vibrational mode of the TST saddle point involves substantial movement for both the transferred hydrogen (H_{13}) and the retained hydrogen (H_{14}) while other atoms remain almost static (Figure 3 and animation file in the Supporting Information). For bound vibrational modes, the energy states are quantized (e.g., zero point energy) and proportional to the vibrational frequency (which is sensitive to both the "force constant" arising from the bonding environment and the mass of atoms involved in the mode); while for the unbound vibrational mode the deviation from classical behavior is manifested as the tunneling effect.[7] In KIE theories, quantum tunneling is predicted to have profound impact on 1° KIE but (often) negligible effect on 2° KIE, assuming the transferred hydrogen (1° hydrogen) is involved in the reaction coordinate (unbound degree of freedom), while the motion of other atoms (2° hydrogens) are contained in the orthogonal coordinates (Figure 5).[15,16] In this case, however, not only the transferred hydrogen but also the retained hydrogen is involved in the reaction coordinate. As a result, both 1° KIE and 2° KIE are significantly impacted by tunneling effect in the Chugaev elimination reaction. This coupling of 2° hydrogens to the reaction coordinate is not unprecedented, and some examples are discussed in the next section. In this study, the SCT model provides best agreement with experimental KIEs as it deals with the "corner-cutting" effect in which the system tunnel under the MEP, and it is generalized to deal with many-dimensional systems that have coupling of the reaction coordinate to orthogonal coordinates.[45]

2.5. Discussion in the Context of Related Research.

Measuring intramolecular KIE of the singly labeled substrate at a methylene group is a frequently applied method by organic

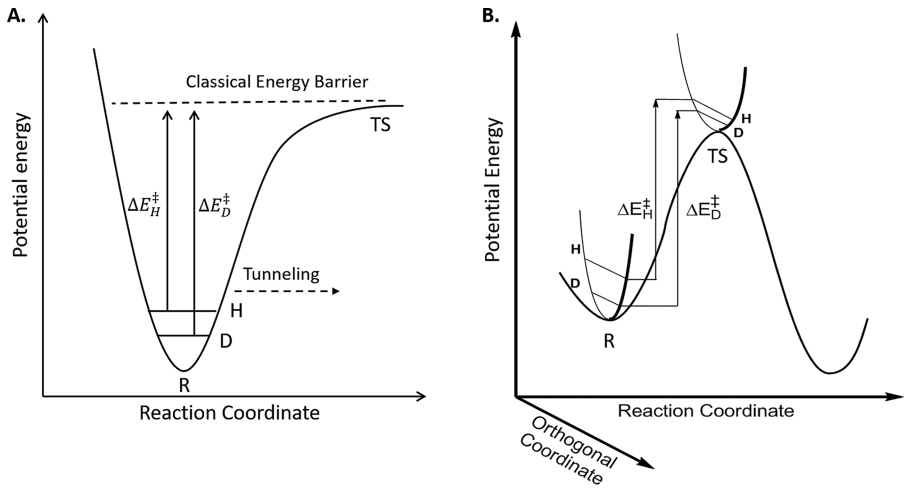

Figure 5. (A) Simple semiclassical model for primary/secondary H/D KIEs resulting from the difference in zero-point energies contained in the reaction coordinate. (B) H/D KIEs originating from zero-point energy differences at the reactant (R) and transition state (TS) in vibrational modes orthogonal to the reaction coordinate leading to a smaller activation energy $\Delta E_H^{\ddagger}$ relative to $\Delta E_D^{\ddagger}$. Further rate enhancement occurs through tunneling into the classically forbidden region under the barrier, and it is related in part involved in the curvature of the reaction coordinate in the region of the TS as well as the mass of the hydrogen (H tunneling more effectively than D).[15,16]

DOI: 10.1021/acs.jpca.9b00172
J. Phys. Chem. A 2019, 123, 3647–3654

chemists to study reaction mechanisms.[53−56] Unfortunately, this study implies that caution should be used when using intramolecular KIE to interpret reaction mechanisms, since some important information such as tunneling effects may not be revealed by intramolecular KIE, especially for elimination reactions.

There have been research efforts to study the tunneling effect upon secondary KIE in elimination reactions before this work. Saunders[57] reported a study on the tunneling contribution to the secondary isotope effect in 1984, and his model calculation study on E2 elimination reaction indicated that the extent of secondary KIE reflects the extent of the contribution of the nontransferred β-hydrogen (the hydrogen on the carbon adjacent to the leaving group) to the motion along the reaction coordinate. What we observe in Chugaev elimination reaction (an intramolecular syn-β-elimination) agrees with what Saunders has found in E2 elimination. Intramolecular syn-β-elimination reaction is similar to E2 reaction in every way except that the base is on the same molecule as the leaving group and the transition state structure is cyclic. The nontransferred β-hydrogen in both E2 and syn-β-elimination reaction undergoes sp^3 to sp^2 rehybridization, resulting in significant motion in the reaction coordinate. More recent computational study by Borden[58] predicts significant tunneling effect in the reductive elimination of methane from an organo-platinum complex, resulting in violation of the rule of geometric mean and a large secondary KIE in the methyl group on the complex due to the motion of the methyl hydrogens in the imaginary vibrational mode. While the previous two works are computational studies, this work provides solid experimental evidence for quantum inflation of the secondary KIE.

Over 3 decades ago, a series of papers by Harold Kwart addressed a wide variety of intramolecular *syn*-β-eliminations using the temperature dependence of intramolecular H/D KIEs.[55,56,59−64] Kwart (and more recently others[65]) have generated linear Arrhenius plots for all systems studied. One aspect of his work, specifically highlighted by Kwart, was the low magnitude of many of the intramolecular KIEs. This feature was attributed to a "bent" hydrogen transfer transition state. While such a scenario might explain Kwart's results in part, work on other systems begin to illustrate that other factors may contribute to reduce intramolecular KIEs in *syn*-β-eliminations. In particular, recent work in Meyer's laboratory yielded an upward concave Arrhenius plot for the pericyclic *syn*-β-elimination in the Swern oxidation of benzyl alcohol.[66] The intramolecular H/D KIE for the Swern oxidation of benzyl alcohol is abnormally low (2.53 at −78 °C). The exceptionally low intramolecular H/D KIE for the Swern oxidation could be due to an abnormally low primary KIE, or an abnormally high secondary KIE, or both in concert. Unfortunately, in the Swern oxidation, the rate-determining step occurs prior to proton abstraction at the methylene in benzyl alcohol, so it is impossible to extract the information necessary to isolate the primary and secondary H/D KIEs. The Chugaev elimination, by contrast, has been shown to occur via rate-limiting hydrogen transfer.[36,37] Thus, we are able to extract primary and secondary KIEs from experimental intra- and intermolecular KIEs. Our results reveal that the quantum amplification of the secondary KIE is the cause of the suppression of the intramolecular KIE in Chugaev elimination. This finding suggests a possible explanation for Kwart's results.

It should be mentioned that an E1 or E1cb mechanism is highly unlikely to give rise to the results presented here. While solvolysis mechanisms can give rise to large secondary H/D KIEs, the rate-limiting step for an E1 mechanism is formation of a carbocation at the carbon which is at the β-position relative to the benzene ring. The substantial 1°and 2° KIEs that manifest at the α-position would be unlikely. Further, the rate-limiting step for an E1cb mechanism is proton abstraction. Aside from being chemically improbable, this mechanism would most plausibly be expected to yield a significant 1° KIE in conjunction with a negligible 2° KIE. These expectations along with previous ^{13}C KIE studies[36,37] reinforce our assertions that neither of the above stepwise mechanisms are relevant to the Chugaev elimination studied here.

The contamination of intramolecular KIE by secondary KIE is less problematic for studies of enzymatic hydrogen transfer reactions, as the primary and secondary KIE are separable and can be measured directly in enzymatic reactions. This is because the substrates are chiral, and the enzymes are naturally stereoselective, e.g., alcohol dehydrogenase reaction,[22] reductive half-reaction of morphinone reductase involving NAD+ and FMN,[67] etc. Experimental and computational evidence of significant tunneling in secondary KIE in enzymatic systems has been reported in NAD^+/NAD-dependent dehydrogenases.[20]

3. CONCLUSION

In summary, this work presents insightful experimental and computational results that can serve as benchmark data for the development of more comprehensive hydrogen transfer theories. We have demonstrated three features of isotope effects in the Chugaev elimination. First is the seemingly classical Arrhenius plot corresponding to the intramolecular H/D KIE which masks pronounced quantum behavior. Second is the exalted secondary H/D KIE at 190 and 180 °C. Third is the observation of quantum behavior at high temperatures, some of which has been hinted at in the [1,5]-hydride shift and may be operative in other *syn*-β-eliminations as a result of the cyclic nature of their transition structures and their substantial reaction barriers.[68−70]

The unimolecular, cyclic transition states which govern *syn*-β-eliminations are likely to find parallels in hydrogen transfer steps in modern reactions of synthetic utility, e.g. those which implement (or suffer from) β-hydride eliminations and numerous intramolecular C−H functionalizations.[53,71−75] We hope that studies such as the one described here can both stimulate the development of new theoretical treatments of hydrogen transfer which can treat both primary and secondary motion in a quantum framework and help to encourage the search for such anomalous behaviors in synthetically and biologically relevant hydrogen transfer reactions.

■ ASSOCIATED CONTENT

Supporting Information

The Supporting Information is available free of charge on the ACS Publications website at DOI: 10.1021/acs.jpca.9b00172.

Synthesis and characterization of **1**, D_1-**1**, and D_2-**1** experimental procedures for measuring KIEs, table of intra- and intermolecular KIE values, raw NMR integration data, energies and Cartesian coordinates of **1** and the transition structure, POLYRATE.dat file, and

DOI: 10.1021/acs.jpca.9b00172
J. Phys. Chem. A 2019, 123, 3647−3654

POLYRATE output rate constants and transmission coefficients (PDF)
Animation of the transition vector (AVI)

AUTHOR INFORMATION

Corresponding Authors

*(D.M.Y.) E-mail: darrin.york@rutgers.edu.
*(M.P.M.) E-mail: matt.meyer@gmail.com.

ORCID

Xiao Li: 0000-0003-2616-9333
Darrin M. York: 0000-0002-9193-7055

Author Contributions

X.L. performed the KIE measurements, labeled substrate synthesis, and POLYRATE calculations. D.M.Y. provided constructive discussion and guidance in the major revision of the manuscript. M.P.M. designed the research project and performed Gaussian calculations.

Notes

The authors declare no competing financial interest.

ACKNOWLEDGMENTS

We thank Dr. Makenzie Provorse Long for her helpful discussion and advice on using the POLYRATE program. This work was supported by the National Science Foundation (CHE-1058483 to M.P.M.) and National Institutes of Health (GM107485 to D.M.Y.).

REFERENCES

(1) Kohen, A.; Klinman, J. P. Hydrogen Tunneling in Biology. *Chem. Biol.* **1999**, *6* (7), R191−R198.
(2) Meisner, J.; Kästner, J. Atom Tunneling in Chemistry. *Angew. Chem., Int. Ed.* **2016**, *55* (18), 5400−5413.
(3) Markland, T. E.; Ceriotti, M. Nuclear Quantum Effects Enter the Mainstream. *Nature Reviews Chemistry* **2018**, *2* (3), 0109.
(4) Bercaw, J. E.; et al. Hydrogen Tunneling in Protonolysis of Platinum(Ii) and Palladium(Ii) Methyl Complexes: Mechanistic Implications. *J. Am. Chem. Soc.* **2008**, *130* (52), 17654−17655.
(5) Roberts, G. M.; et al. Direct Observation of Hydrogen Tunneling Dynamics in Photoexcited Phenol. *J. Phys. Chem. Lett.* **2012**, *3* (3), 348−352.
(6) Bell, R. P. The Application of Quantum Mechanics to Chemical Kinetics. *Proc. R. Soc. London, Ser. A* **1933**, *139* (838), 466−474.
(7) Bell, R. P. Physical principles and early history. *The Tunnel Effect in Chemistry* **1980**, 1−105.
(8) Soudackov, A.; Hatcher, E.; Hammes-Schiffer, S. Quantum and Dynamical Effects of Proton Donor-Acceptor Vibrational Motion in Nonadiabatic Proton-Coupled Electron Transfer Reactions. *J. Chem. Phys.* **2005**, *122* (1), 014505.
(9) Cukier, R. I. A Theory That Connects Proton-Coupled Electron-Transfer and Hydrogen-Atom Transfer Reactions. *J. Phys. Chem. B* **2002**, *106* (7), 1746−1757.
(10) Kuppermann, A.; Truhlar, D. G. Exact Tunneling Calculations. *J. Am. Chem. Soc.* **1971**, *93* (8), 1840−1851.
(11) Marcus, R. A.; Coltrin, M. E. A New Tunneling Path for Reactions Such as H+H2→H2+H. *J. Chem. Phys.* **1977**, *67* (6), 2609−2613.
(12) Nagel, Z. D.; Klinman, J. P. A 21st Century Revisionist's View at a Turning Point in Enzymology. *Nat. Chem. Biol.* **2009**, *5*, 543−550.
(13) Glowacki, D. R.; Harvey, J. N.; Mulholland, A. J. Taking Ockham's Razor to Enzyme Dynamics and Catalysis. *Nat. Chem.* **2012**, *4*, 169−176.
(14) Layfield, J. P.; Hammes-Schiffer, S. Hydrogen Tunneling in Enzymes and Biomimetic Models. *Chem. Rev.* **2014**, *114* (7), 3466−3494.
(15) Kohen, A. Kinetic Isotope Effects as Probes for Hydrogen Tunneling, Coupled Motion and Dynamics Contributions to Enzyme Catalysis. *Prog. React. Kinet. Mech.* **2003**, *28*, 119−156.
(16) Meyer, M. P. Chapter Two - New Applications of Isotope Effects in the Determination Of organic Reaction Mechanisms. *Adv. Phys. Org. Chem.* **2012**, *46*, 57−120.
(17) Simmons, E. M.; Hartwig, J. F. On the Interpretation of Deuterium Kinetic Isotope Effects in C-H Bond Functionalizations by Transition-Metal Complexes. *Angew. Chem., Int. Ed.* **2012**, *51* (13), 3066−3072.
(18) Knapp, M. J.; Rickert, K.; Klinman, J. P. Temperature-Dependent Isotope Effects in Soybean Lipoxygenase-1: Correlating Hydrogen Tunneling with Protein Dynamics. *J. Am. Chem. Soc.* **2002**, *124* (15), 3865−3874.
(19) Alhambra, C.; et al. Quantum Mechanical Dynamical Effects in an Enzyme-Catalyzed Proton Transfer Reaction. *J. Am. Chem. Soc.* **1999**, *121* (10), 2253−2258.
(20) Huskey, W. P.; Schowen, R. L. Reaction-Coordinate Tunneling in Hydride-Transfer Reactions. *J. Am. Chem. Soc.* **1983**, *105* (17), 5704−5706.
(21) Kurz, L. C.; Frieden, C. Anomalous Equilibrium and Kinetic.Alpha.-Deuterium Secondary Isotope Effects Accompanying Hydride Transfer from Reduced Nicotinamide Adenine Dinucleotide. *J. Am. Chem. Soc.* **1980**, *102* (12), 4198−4203.
(22) Kohen, A.; et al. Enzyme Dynamics and Hydrogen Tunnelling in a Thermophilic Alcohol Dehydrogenase. *Nature* **1999**, *399*, 496−499.
(23) Meyer, M. P.; Tomchick, D. R.; Klinman, J. P. Enzyme Structure and Dynamics Affect Hydrogen Tunneling: The Impact of a Remote Side Chain (I553) in Soybean Lipoxygenase-1. *Proc. Natl. Acad. Sci. U. S. A.* **2008**, *105* (4), 1146−1151.
(24) Olsson, M. H. M.; Mavri, J.; Warshel, A. Transition State Theory Can Be Used in Studies of Enzyme Catalysis: Lessons from Simulations of Tunnelling and Dynamical Effects in Lipoxygenase and Other Systems. *Philos. Trans. R. Soc., B* **2006**, *361* (1472), 1417−1432.
(25) Hatcher, E.; Soudackov, A. V.; Hammes-Schiffer, S. Proton-Coupled Electron Transfer in Soybean Lipoxygenase: Dynamical Behavior and Temperature Dependence of Kinetic Isotope Effects. *J. Am. Chem. Soc.* **2007**, *129* (1), 187−196.
(26) Shiner, V. J.; Fisher, R. D. Alpha-Deuterium Effects on the Rates of Solvolysis of a 2-Adamantyl Sulfonate Ester. *J. Am. Chem. Soc.* **1971**, *93* (10), 2553−2554.
(27) Schneider, M. E.; Stern, M. J. Arrhenius Preexponential Factors for Primary Hydrogen Kinetic Isotope Effects. *J. Am. Chem. Soc.* **1972**, *94* (5), 1517−1522.
(28) Stern, M. J.; Weston, R. E. Phenomenological Manifestations of Quantum-Mechanical Tunneling. Ii. Effect on Arrhenius Pre-Exponential Factors for Primary Hydrogen Kinetic Isotope Effects. *J. Chem. Phys.* **1974**, *60* (7), 2808−2814.
(29) Meyer, M. P.; DelMonte, A. J.; Singleton, D. A. Reinvestigation of the Isotope Effects for the Claisen and Aromatic Claisen Rearrangements: The Nature of the Claisen Transition States. *J. Am. Chem. Soc.* **1999**, *121* (47), 10865−10874.
(30) Zheng, J.; et al. *Polyrate-Version 2008*; University of Minnesota: Minneapolis, MN, 2008.
(31) Stern, M. J.; Weston, R. E. Phenomenological Manifestations of Quantum-Mechanical Tunneling. I. Curvature in Arrhenius Plots. *J. Chem. Phys.* **1974**, *60* (7), 2803−2807.
(32) Bigeleisen, J. Statistical Mechanics of Isotopic Systems with Small Quantum Corrections. I. General Considerations and the Rule of the Geometric Mean. *J. Chem. Phys.* **1955**, *23* (12), 2264−2267.
(33) Decius, J. C.; Wilson, E. B. Sum Rules for the Vibration Frequencies of Isotopic Molecules. *J. Chem. Phys.* **1951**, *19* (11), 1409−1412.
(34) Amin, M.; Price, R. C.; Saunders, W. H. Tunneling in Elimination Reactions. Tests of Criteria for Tunneling Predicted by Model Calculations. *J. Am. Chem. Soc.* **1990**, *112* (11), 4467−4471.

DOI: 10.1021/acs.jpca.9b00172
J. Phys. Chem. A 2019, 123, 3647−3654

(35) Saunders, W. H. Calculations of Isotope Effects in Elimination Reactions. New Experimental Criteria for Tunneling in Slow Proton Transfers. *J. Am. Chem. Soc.* **1985**, *107* (1), 164−169.
(36) Bader, R. F. W.; Bourns, A. N. A Kinetic Isotope Effect Study of the Tschugaeff Reaction. *Can. J. Chem.* **1961**, *39* (2), 348−358.
(37) DePuy, C. H.; King, R. W. Pyrolytic Cis Eliminations. *Chem. Rev.* **1960**, *60* (5), 431−457.
(38) Zheng, J.; et al. *Gaussrate-Version 2009-A*; University of Minnesota: Minneapolis, MN, 2010.
(39) Frisch, M. J., et al. *Gaussian 09*; Gaussian, Inc.: Wallingford, CT, 2009.
(40) Zhao, Y.; Truhlar, D. G. The M06 Suite of Density Functionals for Main Group Thermochemistry, Thermochemical Kinetics, Noncovalent Interactions, Excited States, and Transition Elements: Two New Functionals and Systematic Testing of Four M06-Class Functionals and 12 Other Functionals. *Theor. Chem. Acc.* **2008**, *120* (1), 215−241.
(41) Frisch, M. J.; Pople, J. A.; Binkley, J. S. Self-Consistent Molecular Orbital Methods 25. Supplementary Functions for Gaussian Basis Sets. *J. Chem. Phys.* **1984**, *80* (7), 3265−3269.
(42) Truhlar, D. G.; Garrett, B. C. Variational Transition-State Theory. *Acc. Chem. Res.* **1980**, *13* (12), 440−448.
(43) Truhlar, D. G.; Garrett, B. C. Variational Transition State Theory. *Annu. Rev. Phys. Chem.* **1984**, *35* (1), 159−189.
(44) Lu, D.-h.; et al. Polyrate 4: A New Version of a Computer Program for the Calculation of Chemical Reaction Rates for Polyatomics. *Comput. Phys. Commun.* **1992**, *71* (3), 235−262.
(45) Skodje, R. T.; Truhlar, D. G.; Garrett, B. C. A General Small-Curvature Approximation for Transition-State-Theory Transmission Coefficients. *J. Phys. Chem.* **1981**, *85* (21), 3019−3023.
(46) Truhlar, D. G.; Isaacson, A. D.; Garret, B. C., Generalized Transition State Theory. In *Theory of Chemical Reaction Dynamics*; Baer, M., Ed.; CRC Press: Boca Raton, FL, 1985; Vol. 4, pp 65−137.
(47) Garrett, B. C.; et al. Application of the Large-Curvature Tunneling Approximation to Polyatomic Molecules: Abstraction of H or D by Methyl Radical. *Chem. Phys.* **1989**, *136* (2), 271−293.
(48) Pu, J.; Gao, J.; Truhlar, D. G. Multidimensional Tunneling, Recrossing, and the Transmission Coefficient for Enzymatic Reactions. *Chem. Rev.* **2006**, *106* (8), 3140−3169.
(49) Peles, D. N.; Thoburn, J. D. Multidimensional Tunneling in the [1,5] Shift in (Z)-1,3-Pentadiene: How Useful Are Swain−Schaad Exponents at Detecting Tunneling? *J. Org. Chem.* **2008**, *73* (8), 3135−3144.
(50) Sirjean, B.; et al. Tunneling in Hydrogen-Transfer Isomerization of N-Alkyl Radicals. *J. Phys. Chem. A* **2012**, *116* (1), 319−332.
(51) Pauling, L. Atomic Radii and Interatomic Distances in Metals. *J. Am. Chem. Soc.* **1947**, *69* (3), 542−553.
(52) Houk, K. N.; Gustafson, S. M.; Black, K. A. Theoretical Secondary Kinetic Isotope Effects and the Interpretation of Transition State Geometries. 1. The Cope Rearrangement. *J. Am. Chem. Soc.* **1992**, *114* (22), 8565−8572.
(53) Nguyen, Q.; Sun, K.; Driver, T. G. Rh2(Ii)-Catalyzed Intramolecular Aliphatic C-H Bond Amination Reactions Using Aryl Azides as the N-Atom Source. *J. Am. Chem. Soc.* **2012**, *134* (17), 7262−7265.
(54) Harvey, M. E.; Musaev, D. G.; Du Bois, J. A Diruthenium Catalyst for Selective, Intramolecular Allylic C−H Amination: Reaction Development and Mechanistic Insight Gained through Experiment and Theory. *J. Am. Chem. Soc.* **2011**, *133* (43), 17207−17216.
(55) Janssen, J. W. A. M.; Kwart, H. The Thermal Beta-Cis-Elimination Reaction of Cyclic Sulfoxides and Subsequent Ring Expansion Reactions. *J. Org. Chem.* **1977**, *42* (9), 1530−1533.
(56) Kwart, H.; et al. Transition-State Structures in Sulfoxide and Amine Oxide Thermolysis. *J. Am. Chem. Soc.* **1978**, *100* (12), 3927−3928.
(57) Saunders, W. H. Contribution of Tunneling to Secondary Isotope Effects in Proton-Transfer Reactions. *J. Am. Chem. Soc.* **1984**, *106* (7), 2223−2224.
(58) Datta, A.; Hrovat, D. A.; Borden, W. T. Calculations Find That Tunneling Plays a Major Role in the Reductive Elimination of Methane from Hydridomethylbis(Trimethylphosphine)Platinum: How to Confirm This Computational Prediction Experimentally. *J. Am. Chem. Soc.* **2008**, *130* (9), 2726−2727.
(59) Kwart, H. Temperature Dependence of the Primary Kinetic Hydrogen Isotope Effect as a Mechanistic Criterion. *Acc. Chem. Res.* **1982**, *15* (12), 401−408.
(60) Kwart, H.; Brechbiel, M. Role of Solvent in the Mechanism of Amine Oxide Thermolysis Elucidated by the Temperature Dependence of a Kinetic Isotope Effect. *J. Am. Chem. Soc.* **1981**, *103* (15), 4650−4652.
(61) Kwart, H.; Latimore, M. C. Kinetic Deuterium Isotope Criterion for Concertedness. *J. Am. Chem. Soc.* **1971**, *93* (15), 3770−3771.
(62) Kwart, H.; Stanulonis, J. Assessment of the Thioallylic Rearrangement by a Simplified Technique for High-Precision Measurement of Isotope Effects. *J. Am. Chem. Soc.* **1976**, *98* (13), 4009−4010.
(63) Kwart, H.; Wilk, K. A. Evidence for Proton Tunneling in the Strong Base Catalyzed Elimination Reaction of Beta-Phenylethyl Substrates. *J. Org. Chem.* **1985**, *50* (6), 817−820.
(64) Kwart, L. D.; Horgan, A. G.; Kwart, H. Structure of the Reaction Barrier in the Selenoxide-Mediated Formation of Olefins. *J. Am. Chem. Soc.* **1981**, *103* (5), 1232−1234.
(65) Cubbage, J. W.; et al. Thermolysis of Alkyl Sulfoxides and Derivatives: A Comparison of Experiment and Theory. *J. Org. Chem.* **2001**, *66* (26), 8722−8736.
(66) Giagou, T.; Meyer, M. P. Mechanism of the Swern Oxidation: Significant Deviations from Transition State Theory. *J. Org. Chem.* **2010**, *75* (23), 8088−8099.
(67) Pudney, C. R.; et al. A-Secondary Isotope Effects as Probes of "Tunneling-Ready" Configurations in Enzymatic H-Tunneling: Insight from Environmentally Coupled Tunneling Models. *J. Am. Chem. Soc.* **2006**, *128* (43), 14053−14058.
(68) Liu, Y. P.; et al. Molecular Modeling of the Kinetic Isotope Effect for the [1,5]-Sigmatropic Rearrangement of Cis-1,3-Pentadiene. *J. Am. Chem. Soc.* **1993**, *115* (6), 2408−2415.
(69) Chantranupong, L.; Wildman, T. A. Vibrationally Assisted Tunneling in the [1,5] Sigmatropic Hydrogen Shift in Cis-1,3-Pentadiene. *J. Am. Chem. Soc.* **1990**, *112* (11), 4151−4154.
(70) Shelton, G. R.; Hrovat, D. A.; Borden, W. T. Tunneling in the 1,5-Hydrogen Shift Reactions of 1,3-Cyclopentadiene and 5-Methyl-1,3-Cyclopentadiene. *J. Am. Chem. Soc.* **2007**, *129* (1), 164−168.
(71) Williams Fiori, K.; Fleming, J. J.; Du Bois, J. Rh-Catalyzed Amination of Ethereal Cα−H Bonds: A Versatile Strategy for the Synthesis of Complex Amines. *Angew. Chem.* **2004**, *116* (33), 4449−4452.
(72) Du Bois, J. Rhodium-Catalyzed C−H Amination. An Enabling Method for Chemical Synthesis. *Org. Process Res. Dev.* **2011**, *15* (4), 758−762.
(73) Cheng, Q.-Q.; et al. Copper-Catalyzed Divergent Addition Reactions of Enoldiazoacetamides with Nitrones. *J. Am. Chem. Soc.* **2016**, *138* (1), 44−47.
(74) Xu, X.; et al. Enantioselective Cis-Beta-Lactam Synthesis by Intramolecular C-H Functionalization from Enoldiazoacetamides and Derivative Donor-Acceptor Cyclopropenes. *Chem. Sci.* **2015**, *6* (4), 2196−2201.
(75) Deng, Y.; et al. Hg(Otf)2 Catalyzed Intramolecular 1,4-Addition of Donor−Acceptor Cyclopropenes to Arenes. *Org. Lett.* **2015**, *17* (17), 4312−4315.

DOI: 10.1021/acs.jpca.9b00172
J. Phys. Chem. A 2019, 123, 3647−3654